PNAS RESEARCH ARTICLE | CHEMISTRY

Anode electrolysis of sulfides

Jiakang Qu[a], Xiang Chen[a], Hongwei Xie[a], Shuaibo Gao[b], Dihua Wang[b], and Huayi Yin[a,b,1]

Edited by Alexis Bell, University of California, Berkeley, Berkeley, CA; received February 16, 2022; accepted May 21, 2022

Traditional sulfide metallurgy produces harmful sulfur dioxide and is energy intensive. To this end, we develop an anode electrolysis approach in molten salt by which sulfide is electrochemically split into sulfur gas at a graphite inert anode while releasing metal ions that diffuse toward and are deposited at the cathode. The anodic splitting dictates the "sulfide-to-metal ion and sulfur gas" conversion that makes the reaction recur continuously. Using this approach, Cu_2S is converted to sulfur gas and Cu in molten LiCl-KCl at 500 °C with a current efficiency of 99% and energy consumption of 0.420 kWh/kg^{-Cu} (only considering the electricity for electrolysis). Besides Cu_2S, the anode electrolysis can extract Cu from Cu matte that is an intermediate product from the traditional sulfide smelting process. More broadly, Fe, Ni, Pb, and Sb are extracted from FeS, $CuFeS_2$, NiS, PbS, and Sb_2S_3, providing a general electrochemical method for sulfide metallurgy.

sulfide | molten salts | anode electrolysis | desulfurization | green metallurgy

Significance

The pursuit of clean metal production is at the heart of making a sustainable planet. Here, we report an anode electrolysis process that breaks down metal-sulfur bonds at an inert anode to generate sulfur and release metal ions that can be deposited at the cathode in molten salt. In a radical departure from traditional ways, the anode electrolysis electrochemically splits sulfides to metals and sulfur gas without emitting sulfur oxide gases. In this manner, a series of metals was extracted with relatively low energy consumption and cost. If renewable electricity is used as the power, then the anode electrolysis will speed the electrification of sulfide metallurgy to solve the environmental burden and close the metal and sulfur loop.

Sulfide metallurgy is the second largest emitter of SO_2 after coal-fired power plants, which produced 1.23 million tons of SO_2 from the nonferrous metal smelting and pressing industry in China in 2014 (1–3). Many elements exist in the Earth's crust in the form of sulfide minerals such as chalcocite (Cu_2S), chalcopyrite ($CuFeS_2$), galena (PbS), stibnite (Sb_2S_3), bismuthinite (Bi_2S_3), molybdenite (MoS_2), and tungstenite (WS_2) (4, 5). Unlike most transitional metal oxide minerals that can be extracted by carbothermic reduction, the sulfide minerals cannot be reduced by carbon because most sulfides are thermodynamically more stable than CS_2 (6, 7). Instead, the sulfides are treated by matte blowing or converted to oxides that are subsequently reduced by carbon (8, 9). Thus, the extraction of sulfide minerals inevitably produces SO_2 and/or CO_2 that causes severe environmental burdens (10–12). A clean sulfide metallurgy approach is urgently needed to reduce the environmental footprint and to achieve carbon neutralization.

From a chemistry viewpoint, the ideal extraction way is to break down the chemical bonds of metal-sulfur with clean reducing agents (13, 14). In this regard, metal and sulfur are desired products. However, the traditional agent-assisted reduction or oxidation cannot realize this sulfide-to-metal and sulfur conversion. To achieve the goal of producing metal and sulfur, electrochemistry can in principle meet this requirement because the dissociation of sulfide to metal and sulfur involves both reduction and oxidation reactions. The reduction of electrolyte-insoluble sulfides/oxides at the cathode is to remove O^{2-}/S^{2-} from the sulfide/oxide precursors, resulting in the production of metals at the cathode and providing O^{2-}/S^{2-} to the anode that produces O_2 or S_2 (15–17). In addition, molten sulfide electrolysis directly converts molten sulfides to metal and sulfur, but the electrolyte should be engineered to suppress the intrinsic electronic conductivity and decrease the operating temperature to sustain a high current efficiency and guarantee desired anode reactions (18–20). As such, electrometallurgy that uses electric power to drive the dissociation reaction comes to realize this desired conversion, which has been theorized about for a long time (21–24). The success of Al electrolysis demonstrates the power of electrometallurgy that has made significant contributions to our society (25). After the birth of the Hall-Héroult cell, tremendous efforts have been made to find an oxygen-evolution inert anode to generate O_2 rather than CO_2, although there is still no cost-affordable inert anode after more than 100 y of research (26–30). In addition to the work with Al, many attempts have been made to electrochemically split other oxides/sulfides to metals and oxygen/sulfur in various molten salt systems (the schematic diagrams and reaction mechanism are shown in *SI Appendix*, Figs. S1 and S2 and Table S1) (31–35). However, unlike the Hall-Héroult cell, in which Al_2O_3 is soluble in molten cryolite, most oxides and sulfides are insoluble or have a low solubility in molten salt (5). Consequently, the electrochemical reduction of solid/liquid oxides or sulfides will produce insoluble metal that covers the oxide/sulfide feedstock, which results in relatively slow reduction kinetics (15). However, a low-cost inert anode is still absent in

Author affiliations: [a]Key Laboratory for Ecological Metallurgy of Multimetallic Mineral of Ministry of Education, School of Metallurgy, Northeastern University, Shenyang 110819, P. R. China; and [b]School of Resource and Environmental Science, Wuhan University, Wuhan 430072, P.R. China

Author contributions: J.Q., X.C., and H.Y. designed research; H.Y. directed research; J.Q. and X.C. performed research; H.Y. and J.Q. designed experiments; J.Q. and X.C. carried out experiments; H.X., S.G., and D.W. contributed new reagents/analytic tools; J.Q., X.C., H.X., S.G., D.W., and H.Y. analyzed data; H.Y., J.Q., X.C., H.X., and S.G. contributed to analysis and discussion; J.Q. and H.Y. wrote the paper; and H.Y. and D.W. provided supervision, resources, and funding acquisition.

The authors declare no competing interest.

This article is a PNAS Direct Submission.

[1]To whom correspondence may be addressed. Email: yinhuayi@whu.edu.cn.

This article contains supporting information online at http://www.pnas.org/lookup/suppl/doi:10.1073/pnas.2202884119/-/DCSupplemental.

Published July 25, 2022.

the halogen-based molten salts. Therefore, achieving the goal of converting sulfide to metal and sulfur requires an inert sulfur-evolution anode and electrode reactions with facile kinetics.

In this paper, we propose an anode electrolysis process of sulfides in molten LiCl-KCl at 500 °C, in which sulfide was oxidized to sulfur gas while releasing metal ions that were soluble in molten salt and then reduced to metal at the cathode. Unlike the cathodic electrochemical reduction of sulfide in molten salt (36–39), the anodic process released soluble metal ions into the molten salt rather than S^{2-}. Compared with the molten sulfide electrolysis (9, 10), the anode electrolysis used a secondary molten salt electrolyte to decrease the operating temperature and ensure a relatively high efficiency. Thus, the molten salt with a low melting point was chosen without considering the S^{2-} solubility, and the low temperature rendered graphite as a sulfur-evolution inert anode. More important, the anodic process generates volatile sulfur gas and soluble metal ions, which makes the reaction continuous. In other words, the anode electrolysis is leaching metal cations from the sulfide, which is different from the reduction of sulfide at the cathode that is leaching S^{2-} from the sulfide. Here, we verified the feasibility of this anode electrolysis method for several types of metal sulfides, such as Cu_2S, $CuFeS_2$, FeS, PbS, NiS, Sb_2S_3, and Cu matte, and an enlarged-scale electrolysis was executed to prove the potential for a larger production.

Results and Discussion

1.1 Anode Electrolysis of Cu_2Ss. The current sulfide pyrometallurgy involves mineral separation, matte smelting, matte blowing, and metal refining, such as the Cu extraction process (Fig. 1*A*). After matte smelting, the matte blowing process converts Cu_2S to blister Cu at ~1,200 °C through Eq. **1**.

$$Cu_2S + O_2(g) = 2Cu + SO_2(g) \quad [1]$$

For the anode electrolysis process (Fig. 1*B*), the anodic and cathodic reactions are shown in Eqs. **2**–**4**:

$$\text{Anode reaction}: \ Cu_2S\text{–}2e^- = 2Cu^+ + S_2(g) \quad [2]$$

$$\text{Cathode reaction}: \ Cu^+ + e^- = Cu \quad [3]$$

$$\text{Overall reaction}: \ Cu_2S = 2Cu + S_2(g) \quad [4]$$

In principle, the electron breaks down the metal-sulfur bonds by which the metal ions are leached out from sulfide, and S^{2-} gives electrons to the electrode and is converted to sulfur gas. As shown in Fig. 1*C*, condensed sulfur was found from the quartz tube on the top of the anode, and the Cu sponge was collected from the cathode. This process is different from the electrochemical reduction of sulfide in molten salt, which is a cathodic leaching of S^{2-} together with the reduction of metal

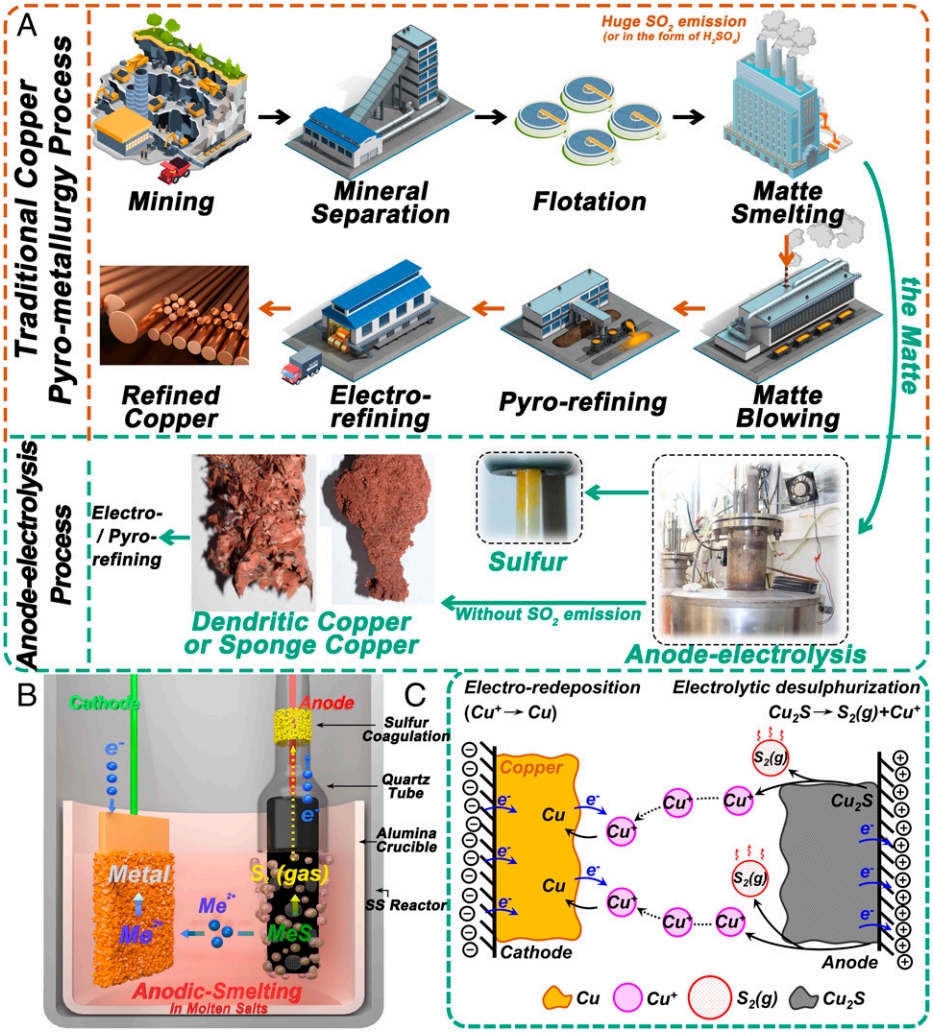

Fig. 1. Schematic illustration of the traditional pyrometallurgy and the sulfide-anode-electrolysis. (*A*) A flowchart of traditional pyrometallurgy and anode-electrolysis process from mining to products (e.g., Cu smelting), (*B*) a schematic diagram of the anode electrolysis system in molten salts, and (*C*) the mechanism diagram of sulfide-anode-electrolysis on the cathode and the anode in this paper.

cations (34). Compared with the oxidative leaching process in aqueous solutions (40), the sulfur gas can leave the electrode instantaneously without forming a sulfur layer that results in the slow kinetics and there is no need to worry about further oxidation of sulfur to sulfate ions. Hence, the combination of the anodic leaching and merit of molten salt enables a straightforward and clean electrochemical sulfide smelting process.

Thermodynamically, the anodic dissolution can happen if the applied potential is lower than the oxidative potential of the anions of molten salt. Otherwise, the anode reaction will exert the discharge of halogen anions (41). As shown in Fig. 2*A* (the pale-blue part), the redox potentials of the Cu-related compounds are within the electrochemical window of the chloride melt, indicating that chloride electrolyte is suitable for the anodic leaching of Cu sulfide without chlorine gas evolution under controlled potential. The thermodynamic oxidation potential of Cu_2S to Cu^+ and S is ~0.6 V more negative than that of the Cl_2 evolution reaction at 500 °C. In addition, the oxide-free molten chloride guarantees the use of graphite as an inert anode that allows the sulfur-evolution reaction. Note that the Cu_2S-to-Cu^+-and-sulfur conversion is thermodynamically more favorable than that of Cu_2S-to-Cu^{2+}-and-sulfur and

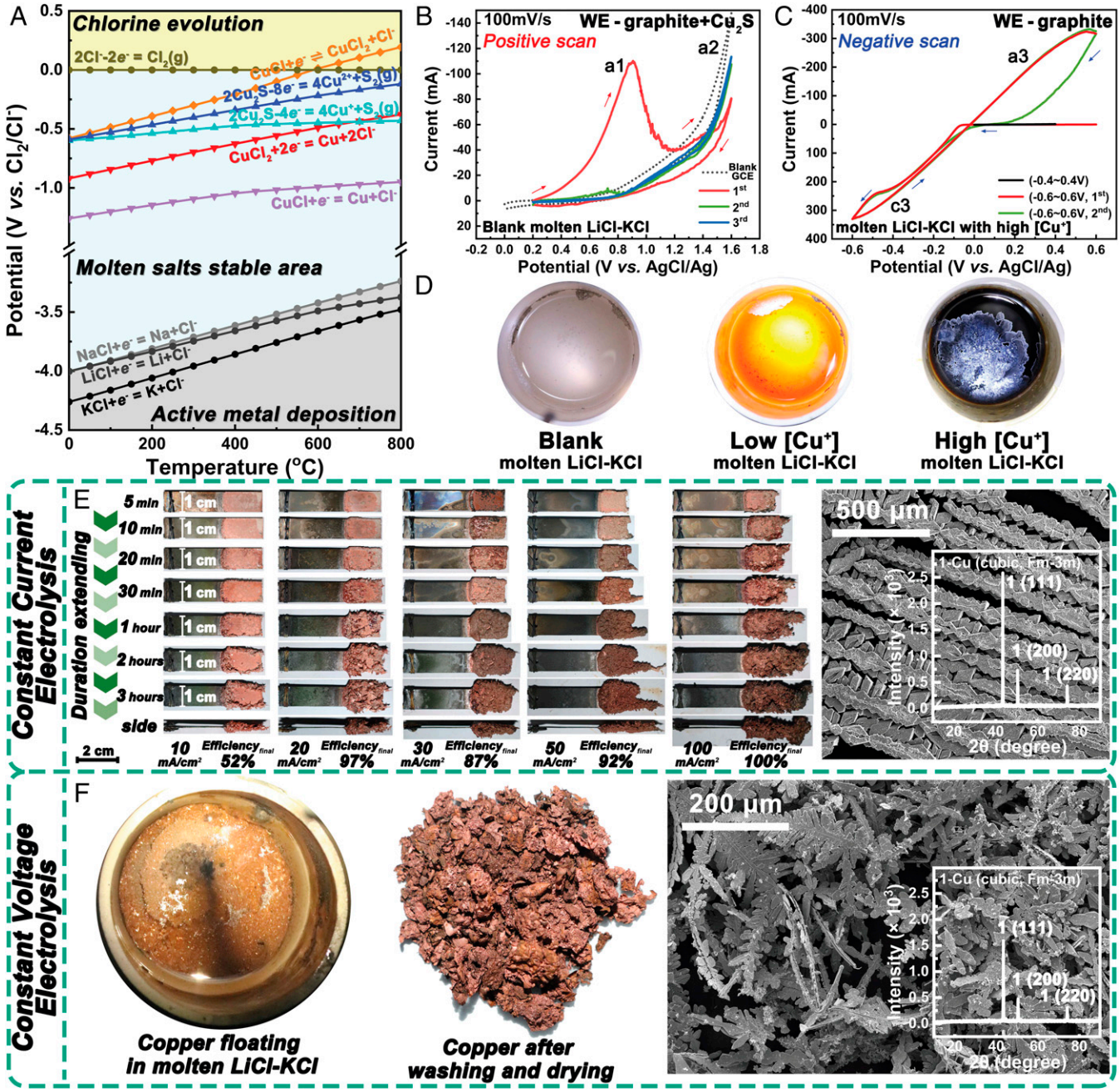

Fig. 2. Thermodynamics and characteristics of CuS anode electrolysis. (*A*) Thermodynamic analysis of CuS electrolysis in pure chloride melts from 0 to 800 °C (the activity of all species are considered the unit (a = 1), and all of the thermodynamic data are obtained from HSC Chemistry 6), (*B*) the first three cycles of positive-scan CV profiles of the graphite cavity working electrode with Cu_2S powders in blank molten LiCl-KCl, (*C*) the first two cycles of negative-scan CV profiles of the blank graphite electrode in molten LiCl-KCl with Cu^+ ions, (*D*) the optical photographs of molten LiCl-KCl with different concentrations of Cu^+ ions, (*E*) optical photographs of deposition products on cathode under different current densities from 5 to 180 min and the corresponding SEM image and XRD pattern, and (*F*) optical photographs of the product floating in the molten LiCl-KCl after constant-voltage electrolysis and the corresponding SEM image and XRD pattern.

$CuCl$-to-$CuCl_2$ conversions. On the cathode side, the deposition potential of Cu is much more positive than that of Li, Na, and K, which has been widely verified (42–45). Hence, the competition reactions at both anode and cathode are negligible in molten salt, which is markedly different from the deposition in the aqueous solution that must compete with the H_2 evolution reaction (46). In addition to Cu_2S, the thermodynamic data of the anodic leaching reactions of other metal sulfides (*SI Appendix*, Fig. S3 and Table S2) show that CuS/Cu_2S, $CuFeS_2$, PbS, Sb_2S_3, FeS, NiS, and Bi_2S_3 can be extracted by the anodic leaching. However, we need to consider the electronic conductivity of the sulfides and the melting points of the derived metal chloride. For example, the chlorides of Mo, W, Sb, and Bi are easy to vaporize at the operating temperature, thereby making the deposition difficult.

As shown in Fig. 2*B*, the oxidation peak a1 started at ∼0.4 V (versus AgCl/Ag, all potentials refer to this reference electrode unless otherwise noted in the paper), which was ascribed to the anodic dissolution reaction (Eq. **2**). The second oxidation peak a2 starting at ∼1.0 V corresponded to the Cl_2 (g) evolution reaction. Thus, the cyclic voltammetry (CV) results agreed well with the thermodynamic calculation. Meanwhile, the oxidation current of Cu_2S dissolution almost disappeared from the second cycle, indicating that the oxidation of Cu_2S on the anode was fast and the Cu_2S powder had been fully dissolved at the first scan. After the Cu_2S was anodically dissolved, the Cu^+ deposition was observed at ∼ −0.1 V (Fig. 2*C*), and the oxidation peak at ∼0 V was the oxidation of Cu to Cu^+. Moreover, two CV profiles in a more positive potential range in the molten salts containing Cu^+ are shown in *SI Appendix*, Fig. S4. A pair of peaks at ∼1.2 V (a2/c2 versus AgCl/Ag), next to the Cl_2 (g) evolution (a3 peak), should come from the redox reactions of Cu^{2+}/Cu^+. The wide potential gap between $\varphi_{Cu+/Cu}$ and $\varphi_{Cu2+/Cu+}$ ensures that Cu^+ prefers to be reduced on the cathode rather than be oxidized on the anode, which avoids a competing reaction and thereby increases the current efficiency of the anode reaction. In addition to CV measurement, the results of two-electrode electrolysis confirmed the success of the anodic leaching and cathodic deposition (Fig. 2*E* and *F*). Before electrolysis, the molten LiCl-KCl was clear and transparent (Fig. 2*D, Left*). After electrolysis, the color gradually changed from orange (after ∼8 g Cu_2S was anodized into the melt as Cu(I), Fig. 2*D, Center*) to dark brown (after ∼30 g of Cu_2S was anodized, Fig. 2*D, Right*). The color change of molten salt should be attributed to the generation and accumulation of CuCl (47, 48), which is verified by the X-ray diffraction (XRD) pattern of the molten LiCl-KCl after electrolysis (*SI Appendix*, Fig. S5). Note that only CuCl was observed, indicating the high selectivity of the anodic leaching reaction. Besides the color change of molten salt, the current efficiency reached 89% after 40 g Cu_2S had been leached into the molten salt (*SI Appendix*, Table S3). The recovery yield is in accord with the change in the current efficiency, which reaches ∼90% with the times of electrolysis. The relatively low current efficiency and recovery yield at the beginning should be due to the low CuCl concentration, which cannot balance the anodic current and thus a side reaction took place. Thus, adding a certain amount of CuCl into molten salt can avoid the side reaction at the beginning of the electrolysis and maintain a high current efficiency from the start.

As shown in Fig. 2*E*, Cu grew on the surface of Ni sheets after constant current electrolysis. As electrolysis proceeded, dendritic Cu with a metallic luster appeared (Fig. 2*E*). The deposition process was also recorded by a camera (Video S1). Moreover, the current efficiency increased with increasing the current density from 10 to 100 mA cm^{-2}. The low current efficiency at low current density could be due to the weak adherence of the electrolytic product to the metal substrate. In addition, the deposition rate increased from 12 mg · cm^{-2} · h^{-1} (10 mA · cm^{-2}) to 246 mg · cm^{-2} · h^{-1} (100 mA · cm^{-2}) (*SI Appendix*, Fig. S6). To our surprise, the deposited Cu tended to float on the surface of molten salts instead of adhering to the substrate under constant cell voltage electrolysis (Fig. 2*F*). The electrolytic Cu showed a brushwood-like structure (Fig. 2*F*), and this "brushwood" Cu can even float above the water (as shown in Fig. 2*F* and Video S2). The micromorphology of this Cu presented a classical fluffy structure with numerous interspaces, and these void spaces rendered the structure able to contain gas and provide enough buoyancy for the Cu to float up. The weak connection with the substrate could be due to the uneven growth rate under constant cell voltages, and the deposition was fast at the beginning. For example, the electrolysis current reached 500 mA · cm^{-2} under 2.0V . The fluctuation of the current-time (I-t) and voltage-time (V-t) curves should be caused by sulfur gas evolution that may cause the anode effect (*SI Appendix*, Fig. S7). Therefore, constant current electrolysis is better for materials collection.

1.2 Anode Electrolysis of Other Metal Sulfides. In addition to Cu_2S, anode electrolysis is an effective approach to extracting other metals from their corresponding sulfides. As shown in Fig. 3*A*, the elements of purple color were extracted from the sulfides, and those highlighted in yellow are thermodynamically feasible to be smelted by this method but have not yet been extracted by the anode electrolysis method. The sulfides before electrolysis (top left corner) and the corresponding metal products (bottom right corner) are shown in Fig. 3*B*. The electrolysis efficiency of each sample is calculated to be >70%, and the efficiency of Cu_2S and high-grade Cu matte can even maintain above 95%. The XRD patterns of these electrolytic products are shown in Fig. 3*C*. For the chalcopyrite, the electrolytic products are Fe, Cu, and $FeCu_4$. In this case, the Fe, Cu, and $FeCu_4$ can be separated by refining procedures afterward or can be used for the preparation of alloys. Meanwhile, some Cu_2O appeared in the electrolyzed chalcopyrite, which should come from the oxidation of the reduced Cu during the washing process. Hence, the SO_2 associated with the FeS-to-FeO conversion can be avoided by this anode electrolysis process.

As shown in the first line of Fig. 3*B*, the electrolytic Cu from CuS/Cu_2S and high-grade Cu matte presented a similar loose structure. As for the low-grade Cu matte and chalcopyrite, the Fe powders with fluffy Cu were collected from the cathode and the bottom of the crucible, which could be separated by magnetic separation or pickling subsequently. For PbS, the anode electrolysis was operated in molten LiCl-KCl at 600 °C, in which $PbCl_2$ has a relatively high solubility at this temperature (49, 50), and electrolytic Pb was liquid and collected in an Al_2O_3 crucible. During electrolysis, small Pb droplets generated first and then small liquid Pb balls aggregated into bigger droplets (as shown in the second line of Fig. 3*B*). Note that the production Pb is helpful for materials collection and continuous operation. For the FeS and NiS, Fe and Ni powders were obtained. Different from the above-mentioned metal sulfides, Sb_2S_3 was anode electrolyzed in molten NaCl-KCl-$AlCl_3$ at 150 °C due to the low boiling point (b.p.) of $SbCl_3$ (b.p. 223.5 °C). Sb powder was obtained (Fig. 3*C*), and the I-t curves of the corresponding electrolysis were shown in *SI Appendix*, Fig. S8. Note that $AlCl_3$ can react with graphite slightly under anodic polarization. Thus, a corrosion-resistant

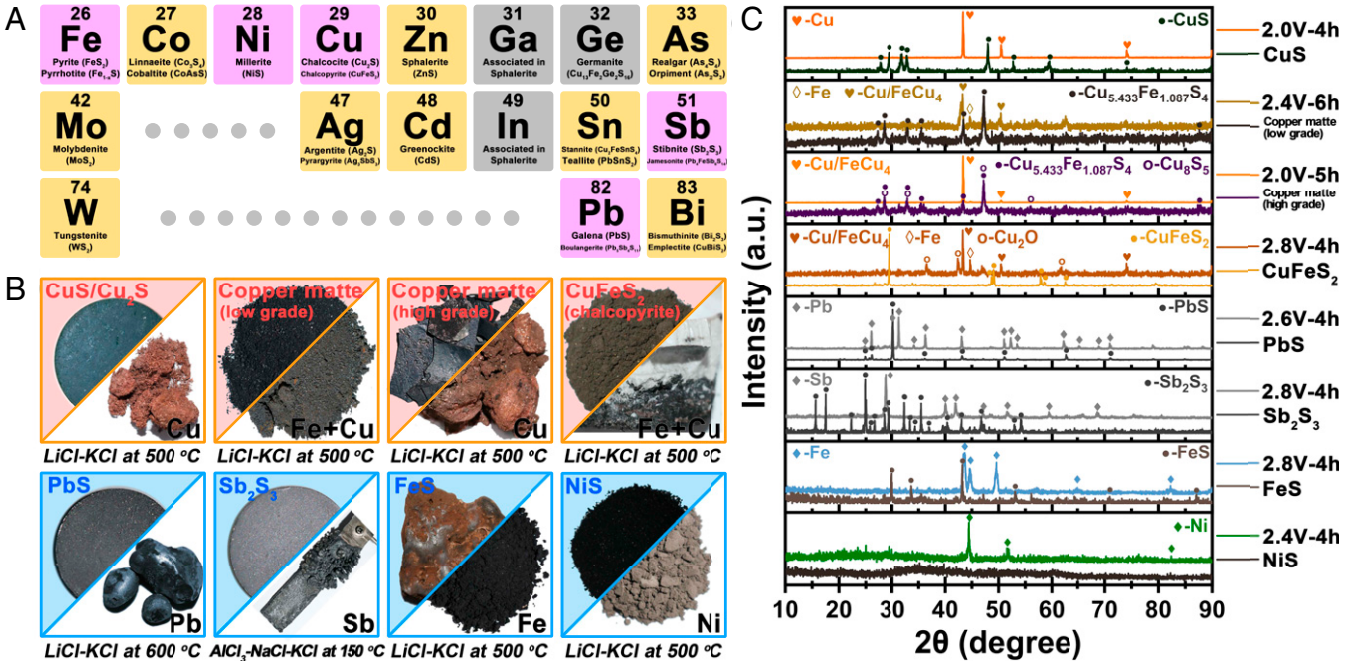

Fig. 3. Typical metals that can be anode electrolyzed practically and theoretically. (*A*) Overview of the metals that have been successfully anode electrolyzed (highlighted in purple) and that are thermodynamically feasible to be smelted by this method (highlighted in yellow), (*B*) digital photographs of several sulfides smelted by the anode electrolysis method, and (*C*) XRD patterns of the sulfides and their corresponding smelted metals.

electrical lead material is a challenge to deploy the anode electrolysis in the $AlCl_3$-based molten salt electrolyte.

1.3 Energy Consumption of Anode Electrolysis. Traditional pyrometallurgy has the advantage of the mature technology and a compact plant but the disadvantage of generating incalculable acid gases or producing a large amount of sulfuric acid as a coproduct (21). Except for the environmental pollution, there is also a huge energy loss from traditional pyrometallurgy. For example, the efficiency of traditional pyrometallurgy of copper is 11.3 to 15.9% and the energy consumption is 15.2 to 23.7 MJ to produce 1 kg Cu (51). Here, we estimated the energy consumption of the anode electrolysis method, as shown in Fig. 4*A*. According to the Chinese national standards for Cu smelting enterprises (GB 21248–2014), the energy consumption of per-kilogram Cu should be <2.77 kWh (the energy consumption only accounts for converting Cu matte to anode Cu). The energy consumed by anode electrolysis was calculated to be 0.420 kWh (from Cu matte to Cu, only the electricity used for electrolysis was considered). We admit that the furnace will consume energy, but the scaled-up process could be self-sustained by the Joule heat that is akin to the Al electrolyzer. The specific calculation process is shown in Fig. 4*A*. In addition to the energy consumption, the molten salts and the "tea infuser" graphite crucible anode can be recycled after a long period of use. The molten LiCl-KCl can be re-electrolyzed to remove the nonactive metal ions (*SI Appendix*, Fig. S9*A*). There was almost no mass loss or oxidation of the tea infuser graphite crucible anode after ~72 h of electrolysis (*SI Appendix*, Fig. S9*B*). The inertness of the graphite anode is due to the relatively low operating temperature and oxide-free environment.

Then, an enlarged-scale anode electrolysis test of high-grade Cu matte was executed at 500 °C in molten LiCl-KCl-CuCl (Fig. 4*B*–*E*). Considering a circumstance more suitable to mass production, the cell was designed as an up-down structure, which consisted of a graphite crucible anode at the bottom and a sheet cathode above. As shown in Fig. 4*C* and *D*, the mass and the yield of the Cu deposits increased with increasing the current density, but there is a drop in the current efficiency caused by the shedding of the rapidly deposited Cu. Even at the lowest efficiency (45.90%, 150 mA · cm^{-2} sample), the energy consumption could meet the standards of traditional pyrometallurgy. The inserted photographs in Fig. 4*E* present the rapid deposition process in this cell, which was cut from Video S3. Thus, the anode electrolysis has the potential to be scaled up.

Conclusions

A sulfide-anode-electrolysis approach has been demonstrated as a clean way to electrochemically split sulfide to sulfur gas and metal in molten salt. At the anode, the sulfide was oxidized to sulfur while releasing metal cations that were reduced to metal at the cathode. A low energy consumption of 0.420 kWh/kg^{Cu} was achieved with a current efficiency of >90%. In addition, Cu, Pb, Fe, Ni, and Sb have been prepared by the anode electrolysis process. The success of sulfide-anode-electrolysis is thanks to the wide electrochemical window that allows the deposition of metals at the cathode and sulfur evolutions at the anode with minimal competition reactions. In addition, the intrinsic properties of the sulfide enable facile kinetics and graphite as an ideal sulfur-evolution inert anode. The enlarged-scale electrolyzer gives us the hope that sulfide-anode-electrolysis is a promising agent-free metallurgical process, not only reducing the toxic gas emissions but also closing the metal and sulfur loop of our planet.

Materials and Methods

Materials. Anhydrous NaCl (analytical reagent [AR] grade 99.5%), KCl (AR 99.5%), $AlCl_3$ (AR, 99%), and LiCl (AR 99.5%) used in this work were purchased from Shanghai Aladdin Bio-Chem Technology. NaCl, KCl, and LiCl were vacuum-dried at 300 °C for 12 h before use. CuS, Cu_2S, PbS, NiS, Sb_2S_3, and FeS powders were purchased from Shanghai Macklin Biochemical. The chalcopyrite and Cu matte were purchased from Jinchuan Group. Graphite rods (spectrum purity, 99.99%) were purchased from Sinosteel Shanghai New Graphite Materials.

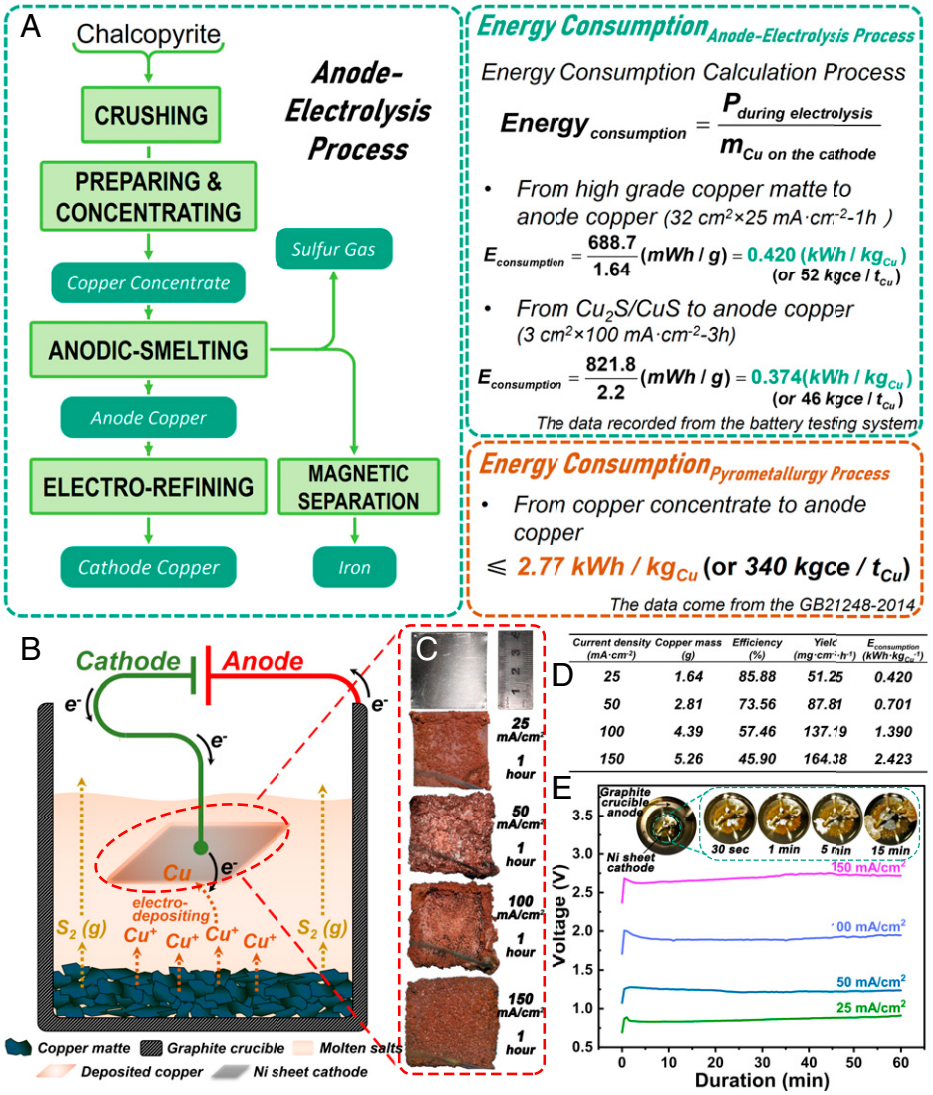

Fig. 4. Energy consumption estimation and the scale-up experiment. (*A*) Simplified subsystems and energy consumption estimation of the anode electrolysis process, (*B*) schematic diagram of the enlarged-scale anode electrolysis cell, (*C*) electrodeposited Cu on the Ni sheet under different current densities after 1 h, (*D*) the table of current efficiency, yield, and energy consumption of different samples, and (*E*) the voltage-time curves of the electrolysis under different current densities (the inserted photographs are the deposited Cu at different durations).

Electrochemical Measurements. First, predried NaCl, KCl, LiCl, and $AlCl_3$ were blended into LiCl-KCl (400 g, LiCl:KCl = 45.6:54.4, wt.%) and NaCl-KCl-$AlCl_3$ (400 g, NaCl:KCl:$AlCl_3$ = 17:17:66, wt.%) mixtures separately in a glove box filled with high-purity Ar gas (>99.999%). Second, the LiCl-KCl mixture was transferred into an alumina crucible and settled in a stainless reactor, which was then heated to 500–600 °C to melt the salt. All of the high-temperature experiments were performed in a stainless-steel (SS) test vessel protected with Ar gas flow (purity: >99.99%, flow rate: 100 mL · min^{-1}). Third, pre-electrolysis was performed between a graphite anode and a Ni sheet cathode at 2.0 V for 4 h to remove the moisture and impurities. Fourth, a three-electrode system connected to an electrochemical workstation (CHI 760E, Shanghai Chenhua Instrument) was used to study the electrochemical behaviors of the metal sulfides in the molten salts by CV. A graphite rod (d = 8 mm) was used as the counter electrode, an Ag wire (d = 1 mm) was used as the quasi-reference, and the homemade graphite cavity electrodes were used as the working electrode to study the reduction and oxidation processes of metal sulfides, respectively, while for the NaCl-KCl-$AlCl_3$, the operating temperature was set at 150 °C and the electrolysis was conducted in a glass chamber protected with Ar gas flow.

Anode Electrolysis of Sulfides in Molten Salts.

Anode preparation. First, a graphite crucible was punched with several holes that were sealed with carbon fiber felts to make a tea infuser graphite crucible. Second, sulfide powders were filled in the tea infuser graphite crucible. During electrolysis, a quartz tube was put on the tea infuser graphite crucible to collect the generated sulfur gas. The optical photographs of the anode are shown in *SI Appendix*, Fig. S10.

Cathode preparation. Two types of cathodes were designed. A Ni sheet (10 × 50 × 1 mm^3) was fixed on an SS rod (d = 2 mm), and an Al_2O_3 sleeve was fixed around the Ni sheet to avoid the potential short circuit. The second type of cathode was the crucible cathode. A hook-shaped SS rod was contained in an Al_2O_3 crucible, which was used to collect the liquid metal products generated at the SS rod. The optical photographs of the two types of cathodes are shown in *SI Appendix*, Fig. S11.

Electrolysis. The setup and molten salt electrolyte were the same as those used for the electrochemical measurement. A two-electrode electrolysis cell comprised the as-prepared cathode and the anode contained sulfide powders. The applied voltage between the two electrodes was supplied by a battery testing system (5V-6A, Shenzhen Neware). Both constant-current and constant-voltage electrolysis were performed. After electrolysis, molten salt and cathode products were collected to study the electrochemical reactions at both anode and cathode.

An enlarged-scale anode electrolysis was also operated, a graphite crucible was directly settled as a container anode, sufficient high-grade Cu matte (150 g) was filled at the bottom of the crucible, and a piece of Ni sheet (40 × 40 × 1 mm^3) was hung in the upper space of the molten salt upon the Cu matte as the cathode. Different current densities were applied on the cell. The same molten LiCl-KCl with preadded CuCl and battery testing system as mentioned above

were used. After electrolysis, the samples were washed and dried for characterizations.

Calculation of the current efficiency. The current efficiency was calculated according to the following formula:

$$\eta_{\text{Electrolysis efficiency}} = \frac{Q_{\text{theoretic}}}{Q_{\text{actual}}}$$

where the $Q_{\text{theoretic}}$ was calculated from the charge (C) required for the reduction of the obtained Cu, and the Q_{actual} was recorded from the battery testing system, representing the actual consumption of electricity.

Materials Characterizations. The electrolytic products obtained under different conditions were characterized by scanning electron microscopy (SEM, FEI Quanta FEG 250), and XRD spectroscopy (Shimadzu X-ray 6000 with Cu Kα radiation at λ = 1.5405 Å). The optical photographs were shot using a digital camera (Canon, 600D).

Data Availability. All of the study data are included in the article and/or *SI Appendix* (XXX).

ACKNOWLEDGMENTS. We are grateful for the financial support from the Fundamental Research Funds for the Central Universities (N2025035, N2025034) and the National Natural Science Foundation of China (52031008).

1. National Bureau of Statistics of the People's Republic of China, Industrial emissions and treatment (2014). www.stats.gov.cn/ztjc/ztsj/hjtjzl/2014. Accessed 11 July 2022.
2. R. M. Hoesly *et al.*, Historical (1750-2014) anthropogenic emissions of reactive gases and aerosols from the community emissions data system (CEDS). *Geosci. Model Dev.* **11**, 369–408 (2018).
3. Ministry of Ecology and Environment of the People's Republic of China, Bulletin of the second national survey of pollution sources" (2020). https://www.mee.gov.cn/xxgk2018/xxgk/xxgk01/202006/t20200610_783547.html. Accessed 16 July 2022.
4. T. Norgate, S. Jahanshahi, Low grade ores - Smelt, leach or concentrate? *Miner. Eng.* **23**, 65–73 (2010).
5. H. Yin, B. Chung, D. R. Sadoway, Electrolysis of a molten semiconductor. *Nat. Commun.* **7**, 12584 (2016).
6. A. Vignes, "Sulfide extraction processes" in *Extractive Metallurgy 2: Metallurgical Reaction Processes* (Wiley, 2013), pp. 255–294.
7. C. Stinn, A. Allanore, Selective sulfidation of metal compounds. *Nature* **602**, 78–83 (2022).
8. F. Habashi, Recent trends in extractive metallurgy. *J. Min. Metall. Sect. B* **45**, 1–13 (2009).
9. S. Sokhanvaran, S. K. Lee, G. Lambotte, A. Allanore, Electrochemistry of molten sulfides: Copper extraction from BaS-Cu_2S. *J. Electrochem. Soc.* **163**, D115–D120 (2016).
10. S. K. Sahu, B. Chmielowiec, A. Allanore, Electrolytic extraction of copper, molybdenum and rhenium from molten sulfide electrolyte. *Electrochim. Acta* **243**, 382–389 (2017).
11. E. A. Olivetti, J. M. Cullen, Toward a sustainable materials system. *Science* **360**, 1396–1398 (2018).
12. D. Raabe, C. C. Tasan, E. A. Olivetti, Strategies for improving the sustainability of structural metals. *Nature* **575**, 64–74 (2019).
13. R. E. Kirchain Jr., J. R. Gregory, E. A. Olivetti, Environmental life-cycle assessment. *Nat. Mater.* **16**, 693–697 (2017).
14. J. B. Zimmerman, P. T. Anastas, H. C. Erythropel, W. Leitner, Designing for a green chemistry future. *Science* **367**, 397–400 (2020).
15. W. Xiao, D. Wang, The electrochemical reduction processes of solid compounds in high temperature molten salts. *Chem. Soc. Rev.* **43**, 3215–3228 (2014).
16. M. S. Tan, R. He, Y. T. Yuan, Z. Y. Wang, X. B. Jin, Electrochemical sulfur removal from chalcopyrite in molten NaCl-KCl. *Electrochim. Acta* **213**, 148–154 (2016).
17. G. Z. Chen, Interactions of molten salts with cathode products in the FFC Cambridge process. *Int. J. Miner. Metall. Mater.* **27**, 1572–1587 (2020).
18. X. L. Ge, X. D. Wang, S. Seetharaman, Copper extraction from copper ore by electro-reduction in molten $CaCl_2$-NaCl. *Electrochim. Acta* **54**, 4397–4402 (2009).
19. A. Allanore, Features and challenges of molten oxide electrolytes for metal extraction. *J. Electrochem. Soc.* **162**, E13–E22 (2015).
20. C. Stinn, K. Nose, T. Okabe, A. Allanore, Experimentally determined phase diagram for the barium sulfide-copper(I) sulfide system above 873 K (600°C). *Metall. Mater. Trans. B Process Metall. Mater. Proc. Sci.* **48**, 2922–2929 (2017).
21. F. Habashi, Copper metallurgy at the crossroads. *J. Min. Metall. Sect. B* **43**, 1–19 (2007).
22. A. Vignes, "Electrometallurgical extraction processes" in *Extractive Metallurgy 2: Metallurgical Reaction Processes* (Wiley, 2013), pp. 87–116.
23. D. Fray, Metallurgy: Iron production electrified. *Nature* **497**, 324–325 (2013).
24. W. D. Judge, J. Paeng, G. Azimi, Electrorefining for direct decarburization of molten iron. *Nat. Mater.* (2021).
25. J. Thonstad *et al.*, "Fundamentals of the Hall-Héroult Process" in *Aluminium Electrolysis* (Aluminium Verlag, 2001), pp. 279.
26. S. Q. Jiao, D. J. Fray, Development of an inert anode for electrowinning in calcium chloride-calcium oxide melts. *Metall. Mater. Trans. B Process Metall. Mater. Proc. Sci.* **41**, 74–79 (2010).
27. H. Y. Yin *et al.*, Capture and electrochemical conversion of CO_2 to value-added carbon and oxygen by molten salt electrolysis. *Energy Environ. Sci.* **6**, 1538–1545 (2013).
28. G. Liu, C. E. Bangs, D. B. Muller, Stock dynamics and emission pathways of the global aluminium cycle. *Nat. Clim. Change* **3**, 338–342 (2013).
29. A. Allanore, L. Yin, D. R. Sadoway, A new anode material for oxygen evolution in molten oxide electrolysis. *Nature* **497**, 353–356 (2013).
30. X. Lu *et al.*, A solid-state electrolysis process for upcycling aluminium scrap. *Nature* **606**, 511–515 (2022).
31. G. Z. Chen, D. J. Fray, T. W. Farthing, Direct electrochemical reduction of titanium dioxide to titanium in molten calcium chloride. *Nature* **407**, 361–364 (2000).
32. U. B. Pal, A. C. Powell, The use of solid-oxide-membrane technology for electrometallurgy. *JOM* **59**, 44–49 (2007).
33. S. Q. Jiao, H. M. Zhu, Electrolysis of Ti_2CO solid solution prepared by TiC and TiO_2. *J. Alloys Compd.* **438**, 243–246 (2007).
34. T. Wang *et al.*, Electrolysis of solid metal sulfide to metal and sulfur in molten NaCl-KCl. *Electrochem. Commun.* **13**, 1492–1495 (2011).
35. S. Licht, Efficient solar-driven synthesis, carbon capture, and desalinization, STEP: Solar thermal electrochemical production of fuels, metals, bleach. *Adv. Mater.* **23**, 5592–5612 (2011).
36. D. Wang *et al.*, Electrolysis of converter matte in molten $CaCl_2$-NaCl. *J. Mater. Sci. Chem. Eng.* **6**, 1–11 (2018).
37. H. W. Xie *et al.*, Electrochemical co-desulfurization-deoxidation of low-grade nickel-copper matte in molten salts. *J. Electrochem. Soc.* **165**, E578–E583 (2018).
38. C. Lv *et al.*, Study on the molybdenum electro-extraction from MoS_2 in the molten salt. *Separ. Purif. Tech.* **258**, 118048 (2021).
39. Y. Y. Guo *et al.*, Electrochemically converting liquid Cu_2S-Sb_2S_3 to liquid Cu_2Sb and sulfur in molten salt at 730°C. *ChemElectroChem* **8**, 4550–4558 (2021).
40. K. M. Deen, E. Asselin, The mineral battery: Combining metal extraction and energy storage. *Joule* **4**, 4–9 (2020).
41. H. Xie *et al.*, Thermodynamic considerations of screening halide molten-salt electrolytes for electrochemical reduction of solid oxides/sulfides. *J. Solid State Electrochem.* **23**, 903–909 (2019).
42. P. Y. Shevelin, N. G. Molchanova, A. N. Yolshin, N. N. Batalov, Electron transfer in an electron–ion molten mixture of CuCl–$CuCl_2$–MeCl (Me=Li, Na, K, Cs). *Electrochim. Acta* **48**, 1385–1394 (2003).
43. I. S. Proskurnev, P. Y. Shevelin, N. G. Molchanova, N. N. Batalov, Electrode processes at the glass carbon/LiCl-CuCl-$CuCl_2$ melt interface. *Russ. Metall.* **2012**, 119–127 (2012).
44. P. Y. Shevelin, A. A. Raskovalov, N. G. Molchanova, An electron transfer in CuCl-$CuCl_2$ melt at different Cl_2 partial pressures. *Ionics* **23**, 3163–3168 (2017).
45. K. Matsumoto, K. Shima, T. Sugimoto, T. Inoue, R. Hagiwara, Generation of elemental fluorine through the electrolysis of copper difluoride at room temperature. *Angew. Chem. Int. Ed. Engl.* **60**, 7887–7892 (2021).
46. A. Vignes, "Hydrometallurgical extraction processes" in *Extractive Metallurgy 2: Metallurgical Reaction Processes* (Wiley, 2013), pp. 1–86.
47. E. Christensen, R. W. Berg, J. H. Von Barner, Copper(I) complex formation in chloride melts. Raman spectroscopic and cryoscopic study. *Polyhedron* **8**, 325–332 (1989).
48. K. Zurowski, Observations on the solid system $CuCl_2$-KCl in the temperature range 293–673 K. *J. Therm. Anal.* **38**, 2369–2375 (1992).
49. A. B. Salyulev, A. M. Potapov, Conductivity of some molten chlorides at elevated temperatures I. Experimental and calculation techniques for $BeCl_2$, $ZnCl_2$, and $PbCl_2$. *J. Chem. Eng. Data* **60**, 484–492 (2015).
50. H. Y. Yin *et al.*, Faradaically selective membrane for liquid metal displacement batteries. *Nat. Energy* **3**, 127–131 (2018).
51. B. Boryczko, A. Holda, Z. Kolenda, Depletion of the non-renewable natural resource reserves in copper, zinc, lead and aluminium production. *J. Clean. Prod.* **84**, 313–321 (2014).